Vahideh Radmard
Department of Mechanical Engineering,
State University of New York at Binghamton,
Binghamton, NY 13850

Ahmad R. Gharaibeh
Department of Mechanical Engineering,
State University of New York at Binghamton,
Binghamton, NY 13850

Mohammad I. Tradat
Department of Mechanical Engineering,
State University of New York at Binghamton,
Binghamton, NY 13850

Cong. H. Hoang
Department of Mechanical Engineering,
State University of New York at Binghamton,
Binghamton, NY 13850

Yaman Yaseen Manaserh
Department of Mechanical Engineering,
State University of New York at Binghamton,
Binghamton, NY 13850

Kourosh Nemati
Future Facilities,
New York, NY 10001

Scott N. Schiffres
Department of Mechanical Engineering,
State University of New York at Binghamton,
Binghamton, NY 13850

Bahgat G. Sammakia
Department of Mechanical Engineering,
State University of New York at Binghamton,
Binghamton, NY 13850

Performance Analysis of Corrosion Resistant Electroless Nickel-Plated Impinging Computer Numerical Control Manufactured Liquid Cooling Cold Plate

More than ever before, data centers must deploy robust thermal solutions to adequately host the high-density and high-performance computing that is in high demand. The newer generation of central processing units (CPUs) and graphics processing units (GPUs) has substantially higher thermal power densities than previous generations. In recent years, more data centers rely on liquid cooling for the high-heat processors inside the servers and air cooling for the remaining low-heat information technology equipment. This hybrid cooling approach creates a smaller and more efficient data center. The deployment of direct-to-chip cold plate liquid cooling is one of the mainstream approaches to providing concentrated cooling to targeted processors. In this study, a processor-level experimental setup was developed to evaluate the cooling performance of a novel computer numerical control (CNC) machined nickel-plated impinging cold plate on a 1 in. × 1 in. mock heater that represents a functional processing unit. The pressure drop and thermal resistance performance curves of the electroless nickel-plated cold plate are compared to those of a pure copper cold plate. A temperature uniformity analysis is done using compuational fluid dynamics and compared to the actual test data. Finally, the CNC machined pure copper one is compared to other reported cold plates to demonstrate its superiority of the design with respect to the cooling performance.
[DOI: 10.1115/1.4054972]

Keywords: direct liquid cooling, single-phase cooling, cold plate, impinging cold plate, electroless nickel-plated heat sink, corrosion resistant cold plate

1 Introduction

As the power of electronic chips continues to grow, so does the amount of energy required to cool them. With high heat information technology equipment becoming more prevalent, data centers are facing heat loads that go far beyond the capacities of traditional cooling systems [1]. In response, data center managers must look for more robust thermal management approaches that can deliver cooling for a heat capacity of approximately 50 kW/rack [2]. Air cooling with computer room air conditioner units and computer room air handler units are the most prevailing and well-established methods in the data center industry. For regular air-cooled data centers, one option for keeping up with high heat density is to selectively apply liquid cooling to high heat generating components like central processing units (CPUs) and graphics processing units (GPUs). This option can be deployed without the need to reduce the computer room air conditioner/computer room air handler temperature set points [3,4]. Thus, a hybrid or liquid-assisted air-cooled design can lower the required cooling power while increasing cooling efficiency. The most viable processor-level solution is a conductive cold plate, which can provide localized cooling to electronics by transferring heat from the device to the liquid. A well-designed cold plate can meet high-heat electronic cooling requirements within their critical temperature range. Based on fluid flow, cold plates can be categorized as parallel or impinging. The cold plate type should be selected based on the system's pressure budget, the thermal performance, and the space limitations of the electronic board [5].

In a pioneering work, Copeland [6,7] developed a one-dimensional analytical model for manifold microchannel heat sinks. The author experimentally confirmed that the proposed analytical model could accurately predict the heat sink's performance at high flow rates. More recently, much effort has been dedicated to investigating the thermal and flow performance of single-phase and two-phase cold plates [8–11]. The flow and heat transfer of rectangular parallel flow microchannel cold plates were numerically and experimentally studied by Qu and Mudawar [12,13]. The authors studied the effects of the channel Reynolds number and thermal conductivity of the solid base on the cooling performance of the cold plate. The effect of geometric parameters, such as channel dimensions, base thickness, fin thickness, and height on the cooling performance of microchannel cold plates was investigated through numerical studies [14–16].

One of the most appealing alternatives for applications with dimensions limits and cases with a reduced pressure drop head is impinging heat sinks. Unaccounted for pressure drops reduce data center efficiency by increasing the required coolant flow rate and consequently the amount of pumping power required to deliver

Contributed by the Electronic and Photonic Packaging Division of ASME for publication in the Journal of Electronic Packaging. Manuscript received January 13, 2022; final manuscript received July 7, 2022; published online August 8, 2022. Assoc. Editor: Ronald Warzoha.

the coolant. In addition, a lower pressure drop value reduces the probability of liquid leakage in the cooling loop. An impinging split flow or top-in/side-exit cold plate supplies the cold coolant at the center of the heat sink and returns heated coolant from the sides. In another means, by splitting the flow into two branches, the channel velocity and flow lengths are reduced by half, so the frictional pressure drop is decreased. Radmard et al. [17–19] found that the impinging cooling device pressure drop can be reduced even more by reducing the height of the extended surface in the central impingement zone without sacrificing the heat transfer. Hadad et al. [20,21] studied the thermohydraulic performance of an impingement microchannel cold plate. The authors found that unlike parallel flow cold plates, impingement cold plates can control the location of the maximum chip temperature depending on the location of the impinging inlet port. Kisitu and Ortega [22] presented a novel physics-based laminar flow model for an impinging microchannel cold plate based on an equivalent parallel channel flow method. The authors showed that the new analytical models can accurately predict the thermal-hydraulic performance of the impinging cold plate over a broad range of parameters. Escher et al. [23] introduced a three-dimensional analytical model to investigate the hydrodynamic and thermal performance of an ultrathin heat sink with optimized impinging slot-jets, microchannels, and manifolds for efficient cooling.

Warm liquid cooling (up to 45 °C) is another approach for increasing the data center efficiency and lowering pressure drop marginally. Warm liquid cooling can minimize pressure drop while also allowing liquid cooling to operate over a larger temperature range. Warm liquid cooling may also significantly lower the power consumption of room air conditioning equipment [16–18]. Addagatla et al. [24] studied hybrid server-level cooling through a combination of warm water in a two OPENU web server. The authors found a noticeable improvement in the total cooling power at higher water inlet temperatures up to 45 °C. Note that one major disadvantage to this type of solution is that any increase in liquid temperature will result in an increase in the corrosion rate of the metal being used [25]. Copper-based cold plates are favored in liquid cooled data centers because of copper's excellent thermal conductivity and good machinability, but like other metals, copper will corrode when exposed to a corrosive environment. Water or water-based coolants are the most popular choices for liquid cooling since they offer superior thermal properties like high heat capacity and high heat transfer coefficients. However, water rapidly dissolves oxygen from the air and makes dionized (DI) water slightly acidic. The presence of H^+ ions and the required oxygen in water will accelerate corrosion in the liquid cooling system. Galvanic corrosion is reported as the most dominant failure mechanism in liquid cooling systems, which happens with the presence of dissimilar metals immersed in an electrically conductive solution [26]. Copper-based cold plates are particularly prone to corrosion in the presence of any cathodic metals such as stainless steel. To reduce galvanic corrosion, subcomponent materials in the cooling loops or wetted materials list should be chosen based on their chemical resistance and compliance with regulatory specifications.

A dissimilarity between the brazing material and copper can also trigger galvanic corrosion. Ultimately, corrosion will have an adverse effect on the cooling performance and mechanical integrity of a system's thermal design. For one thing, it can detrimentally affect the cooling performance of various components. More strikingly, it can initiate failure in the coolant distribution unit (CDU) or the cooling system itself due to the emergence of rust holes, blockages, or coolant leakage. There are several different approaches to reducing the corrosion of metals in liquid cooling systems. Cathodic protection is a technique used to control corrosion by forcing the metal under consideration to be the cathode of an electrochemical cell. It connects the metal to be protected to a more easily corroded metal that acts as a "sacrificial anode" [27]. A second technique is to deploy corrosion inhibitors in the candidate coolant. Corrosion inhibitors are chemical compounds that when added to the coolant will decrease the acid consumption and the corrosion rate of metal that is exposed to the liquid. Inhibitors are typically added in small concentrations to the water-based coolants that are common in data centers [28]. An inhibitor acts via an electrochemical reaction, which proceeds uniformly across the exposed surface of the metal and creates a passivation layer that protects it from corrosion. However, the inhibitor additives penalize the cooling performance of the system by lowering the thermal conductivity of the liquid.

Another common method for enhancing the corrosion resistance of metals is the use of a protective coating. In this approach, a barrier of passive components or paints is created to safeguard the target metal from corrosives. One such technique is electroless nickel plating. This method not only increases the metal's corrosion resistance, but itwill also enhance its strength. Additionally, nickel will raise the cold plate's operating temperature, making it more ideal for high-temperature applications [29]. Shia et al. [30] investigated cold plate corrosion with an inhibited propylene glycol/water mixture using the design of experiments method. The authors showed that the manufacturing process plays an important role in the corrosion of copper cold plates and the corrosion risk can be mitigated by enabling new manufacturing processes and nickel plating to the inside surface of the cold plate.

In this study, the concept of processor-level liquid cooling is studied experimentally and numerically using two novel nickel-plated and pure copper novel computer numerical control (CNC) cold plates. A copper block heater is used to mimic the thermal characteristics of a CPU with uniform heat and a surface area of 1 in. × 1 in. (6.45 cm^2). A liquid cooling loop is designed to test the thermohydraulic performance of the liquid cooling cold plates. The actual test data was compared to the compuational fluid dynamics (CFD) results, and a perfect agreement was shown between the numerical and experimental results. Furthermore, the performance curves of the nickel-plated cold plate are compared to those of a pure copper cold plate, looking specifically at a flow rate. To the best of the authors' knowledge, no previous studies have reported a nickel-plated CNC manufactured cold plate's performance evaluation for a processor-level application. Therefore, the author hopes that this work will open up new research pathways and bring attention to the investigation of novel manufacturing approaches such as CNC machining, electroless nickel coating of fins, and proper inlet/outlet design as a means of increasing heat sink thermal and hydraulic performance and reducing heat sink fin erosion-corrosion. The study highlights the impact of various inlet supply liquid temperatures in terms of case temperature and the pressure drop of the cold plate.

2 Description of Designs

Two CNC machined impinging microfin cold plates have been chosen for this study. The thin fins of this novel cold plate create a large surface area, which subsequently enhances its cooling performance. Generally, there are two methods for manufacturing microfinned heat sinks, either by CNC machining or by skiving. Skived fins are created with a sharp and accurately controlled blade tool. The tool shaves layers of material from a solid block of alloy, leaving it attached at the bottom, and then lifts each layer to create a vertical fin that maintains its attachment to the block at a joint. Skiving helps to eliminate the contact resistance that is present with the solder layer is bonded or brazed heat sinks where there is no joint between the fins and the heat sink base. Additionally, this approach enables the manufacturing of a heat sink with very thin fins and improves the cooling efficiency. While skived fins are the most common approach for manufacturing fin heat sinks, the shapes of the skived fins are not as symmetrical as those made with CNC machining. Manufacturing very thin skived fins might cause insufficient hardness and easy deformation. It is common for skived cold plates to succumb to deformation of up to a quarter of their fins due to the pressure of O-rings and block tops. Consequently, this creates channel blockages and reduces efficiency.

Computer numerical control is another highly flexible approach that enables the construction of complex geometries. Skived fin heat sinks typically have thicker fins than CNC manufactured fins, which means they have a lower heat transfer surface area. This study utilizes an ultrathin CNC finned cold plate to provide the highest possible surface area with a 100 μm fin thickness while retaining the advantages of the CNC approach (Fig. 1). The advantage of CNC machining is that the heat sink fins can be manufactured identically and in perfectly straight parallel rows, with each fin having the same thickness and height (Fig. 2). CNC manufactured cold plates have superior corrosion resistance compared to brazed or welded copper cold plates because they minimize the effect of galvanic corrosion. However, as efficient this technology may be to modern cold plate fabrication, there are possible challenges related to cost, time, and expertise in compare with the traditional skiving method.

The manifold part is made with cast acrylic, which has excellent machinability and high resistance to cracking. Generally, cast acrylic is preferred for building the upper liquid cooling parts rather than extruded acrylics. Extruded acrylic is the common choice due to its low cost and easy manufacturing, but it is prone to stress and fracture, which increases the probability of leakage in the cooling loop. The cast acrylic part of this study cold plate is diamond polished to enable a high optical quality. Most cold plate vendors use buffing or flame polishing to melt the outer layer of material to achieve a glass-like appearance. However, melting the acrylic makes it vulnerable to stress cracking as well as spider webbing from the hydrothermal fluctuations. Another advantage of the diamond polished acrylic of this study cold plate is that it is resistant to discoloration and turning yellow. Two G 1/4 in. style threads are designed for the inlet and outlet ports. The high accuracy of the cast acrylic threads can prevent numerous problems like leaking, cracking, and cross-threading in the cold plate. The integrated impinging design eliminates the need for a cut steel jet plate and, consequently, the possibility of galvanic corrosion caused by steel in the loop. A satin aluminum layer is used between acrylic and copper parts. Two deep grooves are created on the acrylic part to hold the ethylene propylene diene monomer O-rings, prevent leakage, and make assembly fast and accurate. The bottom part includes the spreading base and the heat exchanger. Two cold plates were chosen for this study: a raw copper cold plate and an electroless nickel-plated cold plate. Unlike with electroplated nickel, which is mostly a cosmetic finish, the electroless nickel plating process creates a surface finish with enhanced chemical resistance, mechanical resistance, and excellent fluid lubricity. The electroless nickel-plated cold plate can withstand corrosive coolants such as plain water and even salted water without becoming degraded or flaked. Unlike a nickel-plated heat exchanger, which has a very smooth surface, some flaking can be seen on the raw copper heat exchanger on the edges of its channels (Fig. 3). Electroless nickel-plating of copper heat sink provides a unique combination of corrosion and wear resistance. To prevent a galvanic reaction in large-scale deployments where there is a large quantity of dissimilar wetted metals in the presence of the same electrolyte, it is important to have nickel-plated cold plates. Most water-soluble coolants are electrolytes to some extent, especially when considering contaminants in the loop. The pure copper cold plate's internal corrosion is not an issue in small-scale applications with small quantities of dissimilar wetted metals in the liquid cooling system. But in large scale applications, the corrosion of copper must be addressed. Another benefit of a nickel-plated cold plate is that it provides a mirror-like finish on the surface that can be mounted against the processor, which enables the thermal interface material to flow smoothly between the two layers without entrapping air bubbles. On the other hand, a copper cold plate's mating surface can also be made

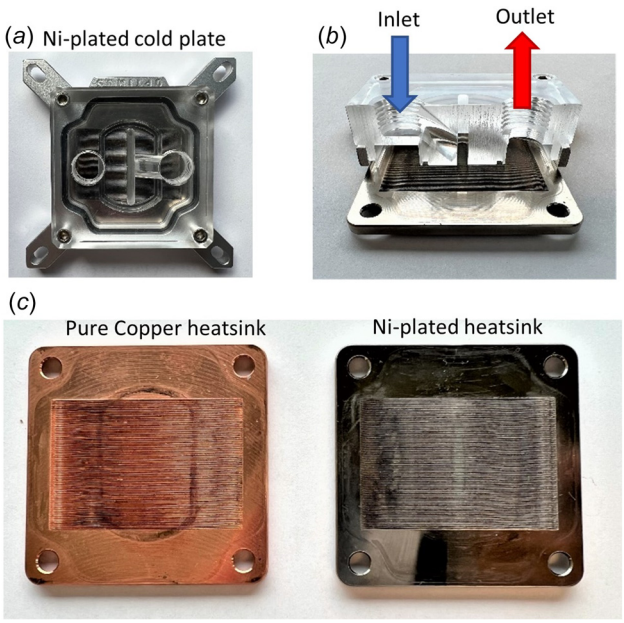

Fig. 1 (*a*) Assembly of the pure copper cold plate, (*b*) channel network and manifold cross section of nickel-plated cold plate, and (*c*) top view of channel network for pure copper and nickel-plated cold plates

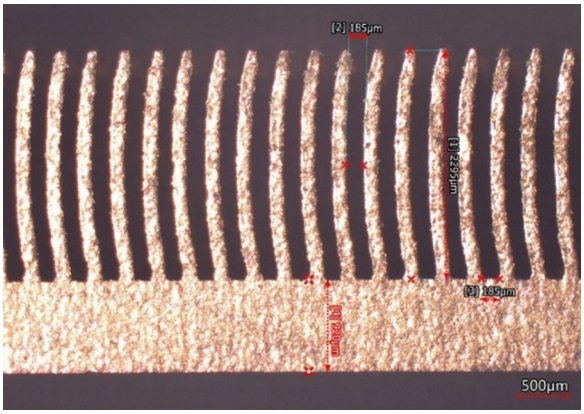

Fig. 2 The cross section image of a pure copper cold plate

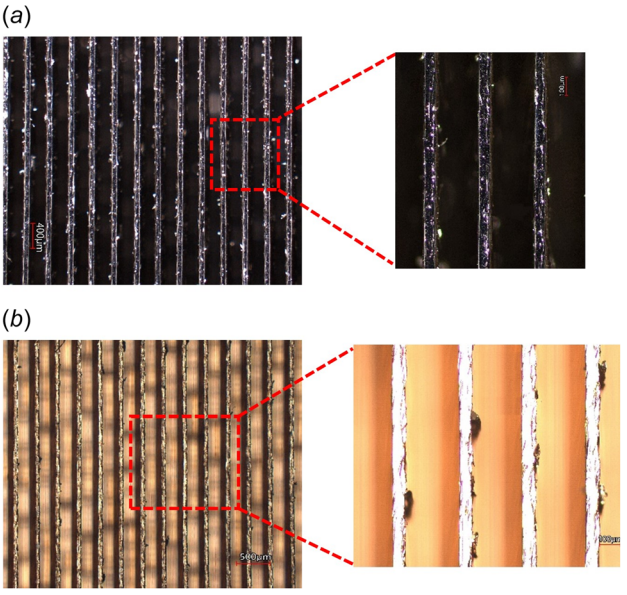

Fig. 3 The SEM of channel network for (*a*) electroless nickel-plated and (*b*) pure copper heat sinks from top view

smooth through polishing, but because it will tarnish upon air exposure it must be done immediately before attachment. The geometric parameters of the cold plates are reported in Table 1.

3 Material Properties

There are several factors to consider when selecting the proper coolant for liquid cooling. A coolant's thermal and hydrodynamic properties are two primary factors to consider. Other possible factors are toxicity, electrical conductivity, *p*H level, flammability, surface tension, bacterial growth, and corrosion. All are major concerns for the reliable and long-term operation of liquid cooling [31,32]. The coolant used for the experimental and numerical analysis of this study is DI water. This coolant has been chosen for its good performance and affordable price. Considering the coolant's importance in the experimental analysis, special attention is given to cleaning the tubes, manifolds, and loops. The material in contact with the coolant is commonly referred to as the wetted material. It is important that material compatibility is established between all the wetted materials and the liquid coolant to prevent and maintain the risk of corrosion at a minimum level. The materials used in each component are usually specified in the manufacturer's product technical data sheet. The ASHRAE TC 9.9 [33] offers a limited list of accepted and avoided recommendation materials for liquid cooling. The component materials used in the cooling loop of this study are listed in Table 2.

Honeywell's PTM7900 (Charlotte, NC) phase change material (PCM) thermal interface material is used between the cold plate and mock processing unit to provide minimum thermal resistance at the interfaces. PCM thermal interface material (TIM) has also been chosen to maintain an excellent performance throughout the reliability testing. The PTM layer ensures excellent interface coverage and wettability during the test, resulting in a much lower contact resistance than thermal grease TIMs. The variation of thermal resistance with pressure has been tested and reported by the manufacturer. The thickness of the TIM decreases when the pressure on the contact surface increases. The pressure applied for the current test is approximately 10 psi, which corresponds to 0.061 K cm^2/W.

4 Experimental Procedures

A benchtop experimental setup was developed to analyze the hydraulic and heat transfer performance of a single cold plate, as illustrated in Fig. 4. A copper block heater with a top surface area of 6.45 cm^2 (1 in. × 1 in.) was utilized to mimic a real processing unit. The copper block heater sufficiently replicates the heat from a high-density heat generating product. Considering its low cost, it was found to be a suitable mock processor candidate for evaluating the thermal performance of the designed cooling solution. Four cartridge heaters were installed onto the copper block heater. Each cartridge heater is rated to deliver up to 400 W. A data center power supply was used to vary the input power of the mock heater through the cartridge heaters. To accurately calculate the heat losses along the heat path to the top surface of the mock heater, three holes were drilled in the copper block, the dimensions of which are shown in Figs. 4(*a*) and 4(*b*). Then, two K-type thermocouples were used to measure the temperature gradient along the copper block. Furthermore, to reduce heat losses due to radiation and natural convection, the copper block was placed in a polystyrene box and all sides except for the top surface were insulated with fiberglass. The cold plate base temperature was reported at two locations by the installed T-type thermocouples in the machined slots at the base. The DI water coolant outflow from the CDU coolant reservoir was driven by a CDU internal pump through the coolant flow loop. The flow rate was varied via the CDU interface by selecting the power level of the pump. To report the coolant volumetric flow rate precisely, an in-house calibrated FTB313D flowmeter with a flow ranging from 0.2 to 2 LPM and an accuracy of 6% of flow sensor was used. The coolant temperature and pressure at the inlet and outlet of the cold plate were measured by attaching T-type thermocouples and OMEGA PX309-050A5V pressure transducers to the cooling loop as shown in Fig. 4(*c*). The range and accuracy of the pressure transducers are –15 to 50 PSIG and ±1%, respectively. A data acquisition (DAQ) system from NI instruments was programed using LABVIEW virtual instrument (VI) to read and export temperature and pressure data to excel documents. The tested cases were performed with a coolant flow rate varying from 0.9 to 1.5 LPM. A summary of the equipment used during the experiment, including model, range, and accuracy per the vendor specification, is presented in Table 3. The copper heater top surface is flat and without discontinuity to generate a uniform heat flux. Two thermocouples were placed at 3.04 mm and 15.74 mm from a top mating surface allows for predicting the case temperature, under the PTM TIM.

In a real chip case (Fig. 5), the total thermal resistance is

$$R_{\text{th}}^{\text{tot}} = R_e + R_i \tag{1}$$

$$R_i = R_{J-\text{case}} + R_{\text{TIM}} \tag{2}$$

The case temperature and junction temperature can be related by Fourier's law

$$\dot{q}_{\text{chip}} = -\text{KA}\,\frac{(T_{\text{case}} - T_j)}{t_{\text{case}}} \tag{3}$$

The case temperature is used to characterize the cold plate through Eqs. (1) and (2).

The proposed test was designed to attain the temperature of the case of a mock processing unit with a 1 in. × 1 in. size

$$R_{\text{th}} = \frac{T_{\text{case}}^{\text{center}} - T_{\text{in}}}{\dot{q}} \tag{4}$$

For the scenario in which the processor is lidded, the junction temperature can be approximated by adding the junction-to-case thermal resistance to the measured case thermal resistance from the actual test at the specified boundary conditions. In addition to thermal resistance, the pressure drop across the cold plate is tested at different flow rates and inlet temperatures. The uncertainties of thermal resistance and pressure drop are calculated using the root sum square method. Equation (5) represents the overall uncertainty from the contributions made by the uncertainties from each variable in the equation, Xi. Each term of Eq. (5) represents the partial derivative of R with respect to X_i, multiplied by the uncertainty interval for that variable

$$\delta R_{\text{th}} = \sqrt{\left\{\sum_{i=1}^{N}\left(\frac{\partial R_{\text{th}}}{\partial X_i} \times \Delta X_i\right)^2\right\}} \tag{5}$$

where N and ΔX are the number of variables and uncertainty of one variable in the thermal resistance equation, respectively. The simplified version of the equation for thermal resistance including all the variables is

Table 1 Geometric parameters of the cold plate

Parameter	Pure copper cold plate	Ni-plated cold plate
Fin thickness (μm)	76	82
Channel width (μm)	232	223
Fin height (mm)	2.29	2.29
Base thickness (mm)	0.7	0.7
Finned area size (mm^2)	45 × 30.5	45 × 30.5
Cold plate spreader size (mm^2)	57 × 57	57 × 57
Inlet/outlet thread diameter (mm)	12	12

Table 2 Wetted material list

Component	Model	Material
Flow sensor	Omega FTB314D	Polyvinylidene fluoride fluro elastomer O-rings
Coolant temperature sensors	T type	Copper wire and Constantan (Cu and Cu-Ni) alloy
CDU	Koolance ALH-2000	Stainless Steel reservoir
Cold plate	Impinging	Copper/nickel plated copper acrylic, aluminum mounting plate
Cold plate fittings	—	Brass
Tubing	Clear	Vinyl

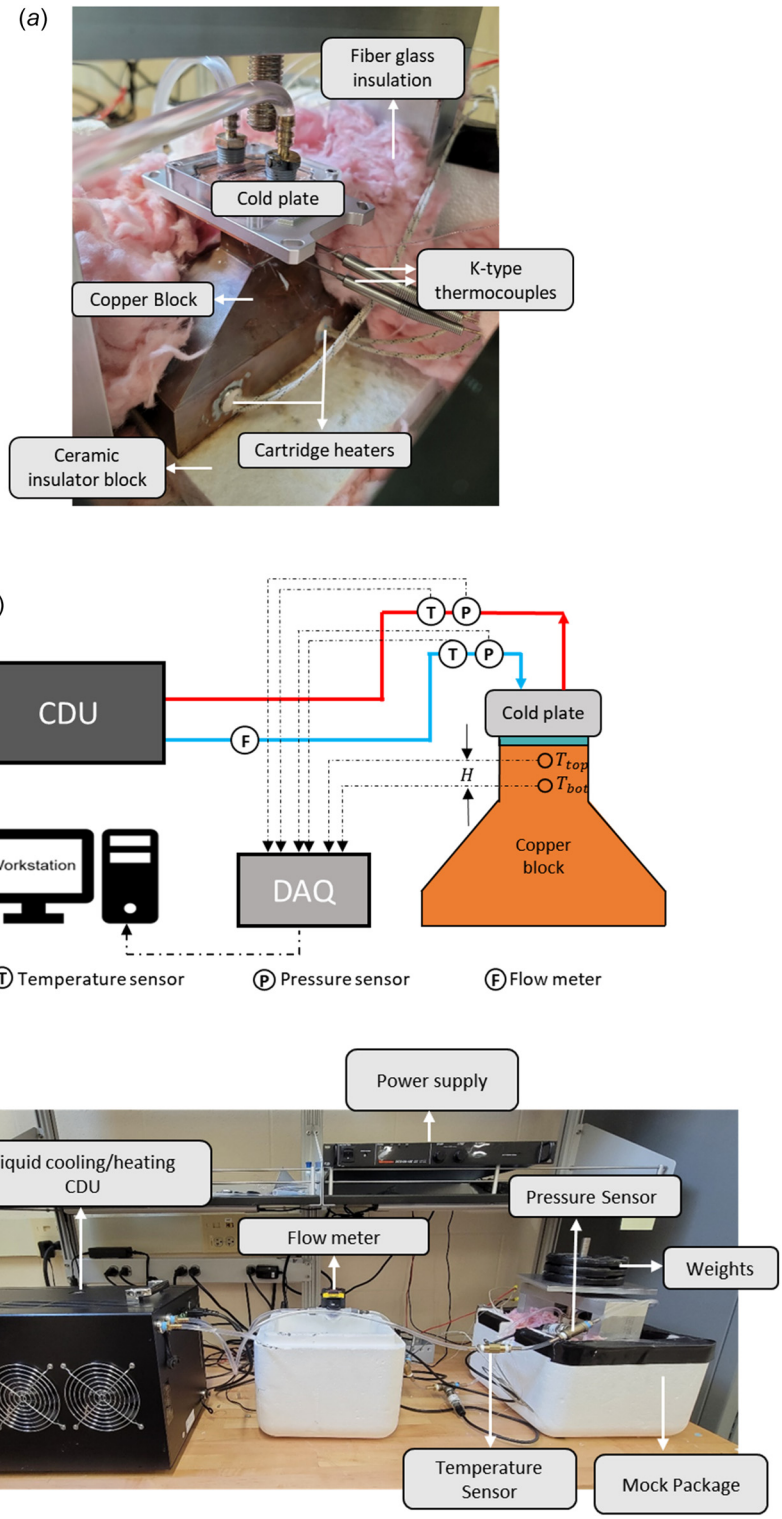

Fig. 4 Benchtop experimental setup (*a*) mock package including the copper block heater and the cold plate, (*b*) schematic of the test setup, and (*c*) benchtop experimental setup

Table 3 Summary of equipment and sensors (model, range, and accuracy)

Equipment	Specification
ALH-2000 CDU	Cooling capacity 2000 W
Thermocouples	T-type (accuracy: ±0.2 °C) K-type (accuracy: ±0.2 °C)
Omega PX3090-50A5V pressure transducer	Accuracy ±0.8 kPa
Omega FTB314D flow sensor	Full scale accuracy: 5%

$$R_{\text{th}} = \frac{(T_{\text{case}}^{\text{center}} - T_{\text{in}}) \times H}{K\,(T_{\text{bot}} - T_{\text{top}})} \tag{6}$$

H is the distance between two K-type thermocouples. The uncertainty equation (Eq. (5)) is applied to the thermal resistance equation (Eq. (6)) with five variables of T_{bot}, T_{top}, T_{in}, $T_{\text{case}}^{\text{center}}$, and H.

The pressure drop uncertainty is obtained from

$$\delta\Delta P = \sqrt{\left\{\sum_{i=1}^{N}\left(\frac{\partial \Delta P}{\partial X_i} \times \Delta X_i\right)^2\right\}} \tag{7}$$

The uncertainty of the pressure sensor (ΔX) used is 0.116 psi.

4.1 Numerical Analysis. Computational fluid dynamics analysis helped in analyzing the impinging cold plate, which was tested experimentally to determine the impact of various water inlet temperatures and nickel coating on the thermal and hydraulic performance of the cold plate. The following assumptions have been made for the numerical governing equations:

(1) Flow is steady-state and single-phase, incompressible, and three-dimensional.
(2) Flow through microchannels is laminar (Re < 211).
(3) The effect of gravity and the thermophysical properties of the coolant are considered.
(4) Radiation heat transfer and viscous heat generation are negligible.

A symmetric view of the computational domain and applied boundary conditions is shown in Fig. 6. The cold DI water is impinged down from the top of the module through the "velocity inlet" and exits from the "pressure outlet." Adiabatic and no-slip boundary conditions are assumed for the current numerical analysis.

No-slip and thermally coupled boundary conditions are applied to the wetted surfaces inside cold plate. PTM TIM thickness is estimated from the conductive thermal resistance equation below:

$$R_t = \frac{t_{\text{TIM}}}{K\,A_{\text{heater}}} \tag{8}$$

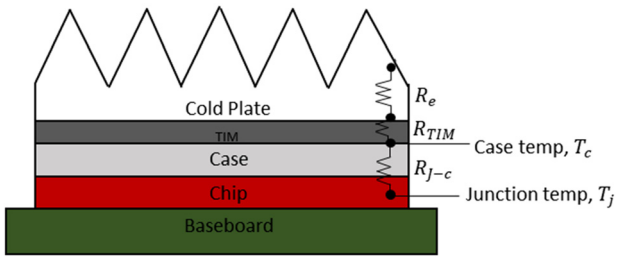

Fig. 5 A schematic of resistances for the heat flow from a real chip to incoming fluid for a regular cold plate arrangement

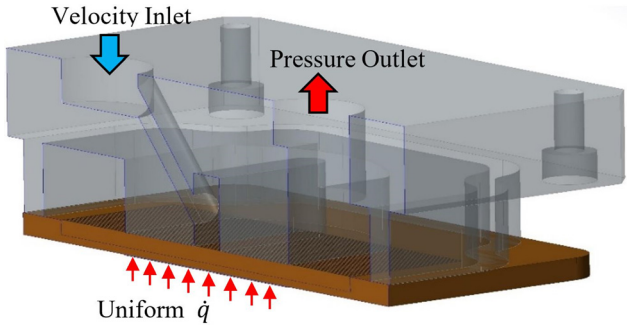

Fig. 6 A symmetric view of the computational domain with applied boundary conditions

For the current heater size, the TIM thickness with a thermal resistance of 0.061 K.cm^2/W and thermal conductivity of 8 W/m K is estimated to be 0.048 mm. Spreading resistance of the TIM is neglected. The numerical study was performed with commercial CFD software 6SIGMAET [34]. The geometry of the copper cold plate imported to CFD included the fin details from the scanning electron microscope (SEM) to reduce the cooling performance uncertainty due to any dimensional mismatch between the vendor reported data and the SEM analysis. The finite volume method is used to discretize the system and to solve the governing equations of continuity, Navier–Stokes, and energy in the defined computational domain. The velocity, pressure, and temperature were predicted using an iterative semi-implicit method for pressure linked equations algorithm. To accurately depict the pressure drop and thermal performance, a structured finer mesh size is implemented in the areas with high temperature and velocity gradients. A grid resolution study is done to find the minimum required grid resolution across the computational domain. Figure 7 shows that increasing the number of cells from 14 to 17×10^6 results in 0.1% and 0.1% variation in the pressure drop and thermal resistance, respectively. All the models reported subsequently were run with at least 14×10^6 number of cells.

5 Results and Discussion

Cold plates are the smallest and most influential subcomponents of the liquid cooling system in a data center. Acquiring accurate cooling performance curves for the cold plate, which is a processor level component, are critical to the server, rack, and data center level analysis. Additionally, pressure testing the cold plate is critical to preventing liquid leaks by maintaining below the available pressure head of the CDU. The cold plates usually have the highest contribution to the total pressure drop of the server level cooling loop. The pressure drop in the current test is obtained in

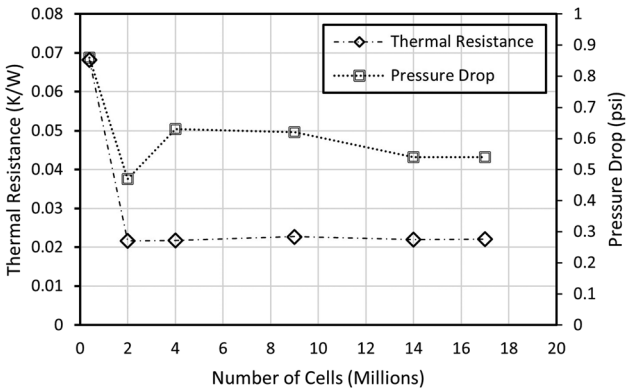

Fig. 7 The results of grid resolution based on thermal resistance and pressure drop

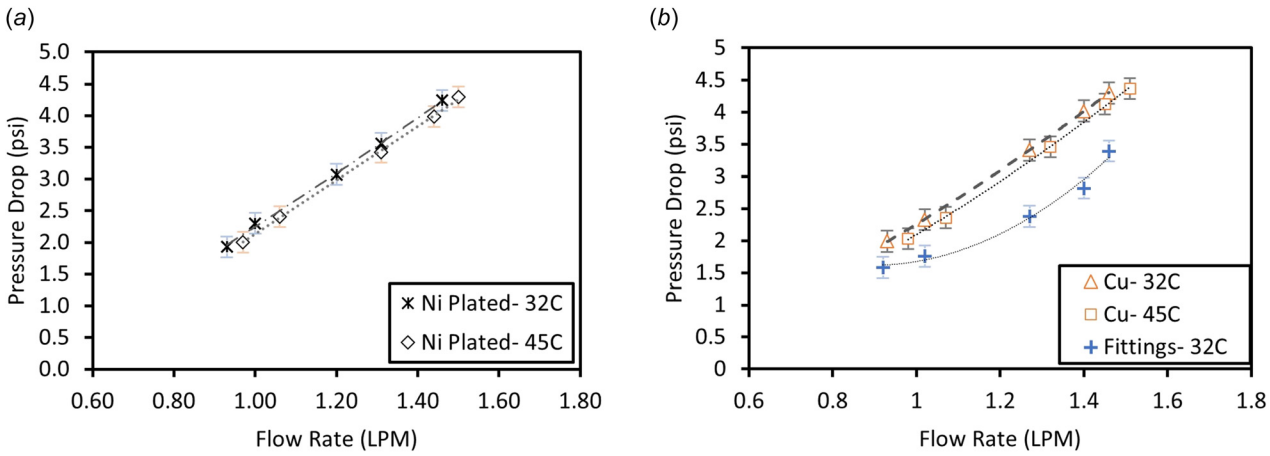

Fig. 8 (*a*) Nickel plated cold plate and (*b*) pure copper cold plate pressure drop curve at two different inlet temperatures of 32 °C and 45 °C

two steps. First, the pressure drop of the fitting and tubes, which are connected to the threaded inlet and outlet ports, is tested at 32 °C. Then, a cold plate pressure drop from the inlet pressure sensor to the outlet pressure sensor is measured at two different inlet temperatures, 32 °C and 45 °C. The high inlet temperature was chosen because of the benefits and popularity of warm liquid cooling in high heat density data centers. Using a higher secondary coolant temperature in a cooling system reduces the chiller energy consumption and, subsequently, increases the design efficiency. The flow in the cooling loop is controlled by varying the pump speed inside the CDU. As can be seen from Fig. 8, the pressure drop of the nickel-plated cold plate (including fittings) is reduced by 6% at 1.45 LPM by increasing the inlet temperature from 32 °C to 45 °C. The same temperature-dependent pressure drop trend is also valid for the pure copper cold plate. Increasing the liquid temperature tends to decrease its viscosity, which increases the pressure drop across the cold plate. By elevating the coolant's inlet temperature, the flow rate in the loop with the same pump speed increases because of the lower total pressure drop in the loop. The electroless nickel-plated microlayer on the finned area, shown in Fig. 3, does not penalize the cold plate's pressure drop. Figure 9 addresses the identical hydraulic performance of nickel-plated cold plate to the pure copper one.

A comparison of the thermal performance for two cold plates is shown in Fig. 10. The electroless nickel plated cold plate is expected to have higher thermal resistance than the pure copper plate since nickel has lower thermal conductivity. According to Fig. 10, the electroless nickel plating slightly increases the case temperature and thermal resistance. The increase in the thermal resistance value is calculated to be 1% at a 32 °C inlet temperature and a 1 LPM flow rate. For a fixed flow rate of 1 LPM, elevating the inlet temperature from 32 to 45 °C decreases the thermal resistance of the copper and nickel-plated cold plates by approximately 2% and 3%, respectively. The lower thermal resistance at a higher inlet temperature is attributed to the fact that the coolant thermal conductivity and specific heat increase with an elevated coolant temperature.

5.1 Computational Fluid Dynamics Analysis. The overall objective is to validate the accuracy of CFD modeling so it can be deployed with certainty for next level analysis and to ensure the results will be reliable for decision-making for design. The experimental test results of the pure copper cold plate are compared with the CFD results. The thermal resistance and pressure drop results obtained by the CFD model are compared with the actual experimental data in Fig. 11. For thermal resistance, the maximum and average discrepancies between the numerical and experimental results are predicted to be 2.8% and 1.3%, respectively. The numerical results indicate that the CFD model is capturing the trend of the experimental results.

The other advantage of CFD modeling is its access to high quality visualization of liquid streams and temperature velocity profiles at specified cross sections in a cold plate. The case temperature profile provides the temperature uniformity analysis of the processor/copper block heater surface. High temperature gradients can induce thermal stresses to the die and other substrates, thus reducing the processors' efficiency and functional lifespan.

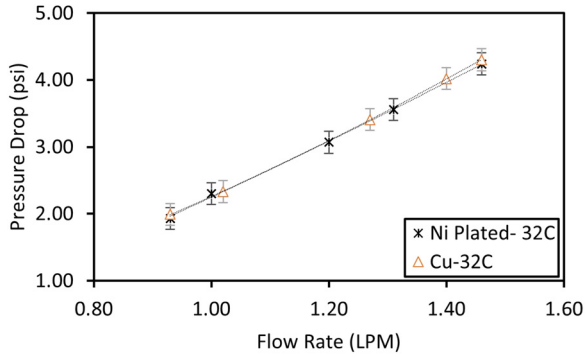

Fig. 9 A comparison of nickel-plated and pure copper cold plate pressure drops at 32 °C. The curves include the fitting's pressure drops.

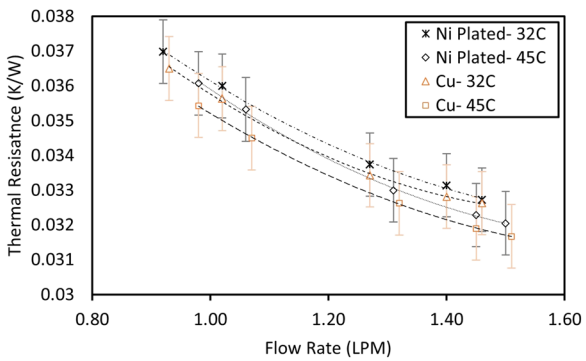

Fig. 10 A comparison of the nickel-plated and pure copper cold plate thermal resistances at various inlet temperatures

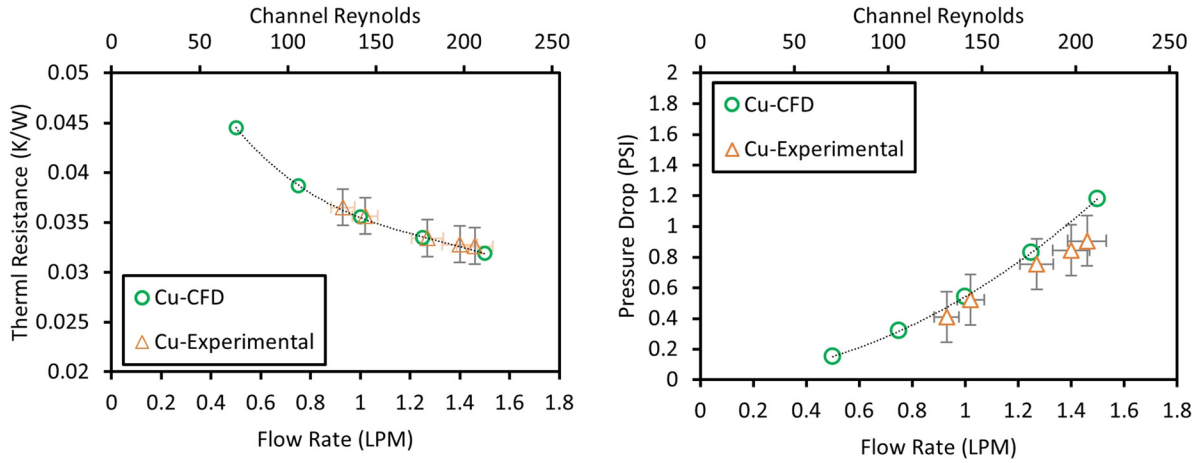

Fig. 11 CFD results compared to actual test data for the pure copper cold plate

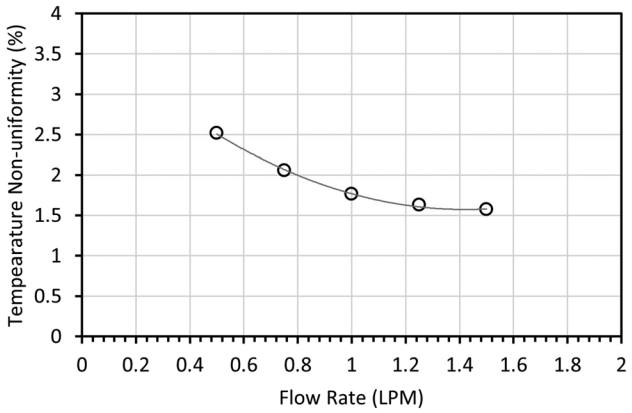

Fig. 12 Temperature nonuniformity on the case profile according to flow rate

The temperature distribution nonuniformity of the chip (Ψ) is used to address temperature uniformity on the processor/copper heater surface. It is defined by

$$\Psi = \frac{\sqrt{\sum_{n=1}^{N} \frac{(T_n - T_{\text{ave}})^2}{N-1}}}{T_{\text{ave}}} \times 100 \tag{9}$$

where N is the number of sensors uniformly distributed on the processor/copper heater surface. In the current CFD study, 49 temperature sensors are placed on the surface of the heater. In an actual test, it is nearly impossible to install 49 sensors on the heater surface. However, CFD allows the desired number of sensors to be placed on the processor. The higher the value of Ψ that the profile has, the more nonuniform its temperature distribution becomes. The temperature profile will become more uniform when the flow rate is increased, as shown in Fig. 12. This can be attributed to the fact that a higher flow rate has a smaller fluid temperature gradient and lower outlet temperature, which will cool the hot areas on the processor/copper heater surface (Fig. 13).

The unsymmetrical location of the outlet port forces more flow streams to form on the side of the cold plate outlet. Figure 14 shows the velocity profile inside the cold plate channels, which illustrates the flow nonuniformity happening inside the cold plates. The more flow that the channels receive, the lower the temperature is on the processor/copper heater surface. In addition to that, the center of the profile uses the advantages of the higher heat transfer coefficient at the impinging slot and remains at lower temperatures. The unfinned area in which the flow streams circulate to reach the outlet port shows the highest temperature.

5.2 Comparison. For a better understanding of the current CNC cold plate superior performance, the pure copper cold plate is compared to other cold plates that have been presented in the technical literature. For an overall comparison, Table 4 provides

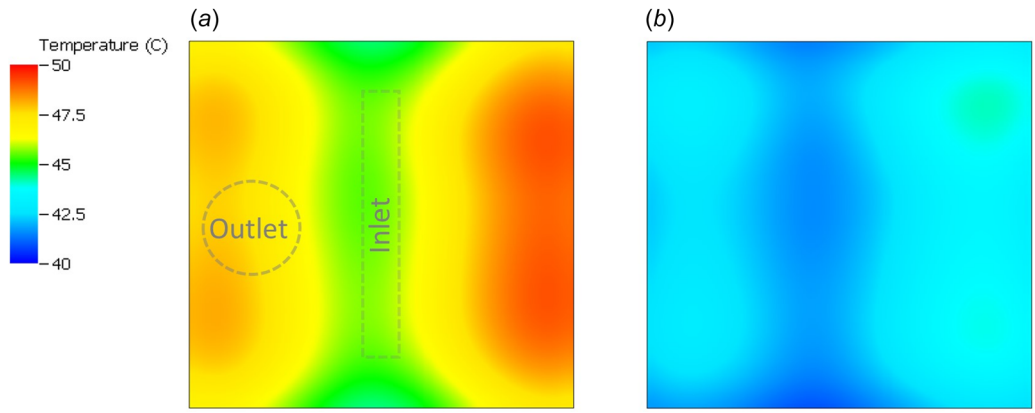

Fig. 13 Temperature profile of the case surface at (*a*) 0.5 LPM and (*b*) 1.5 LPM

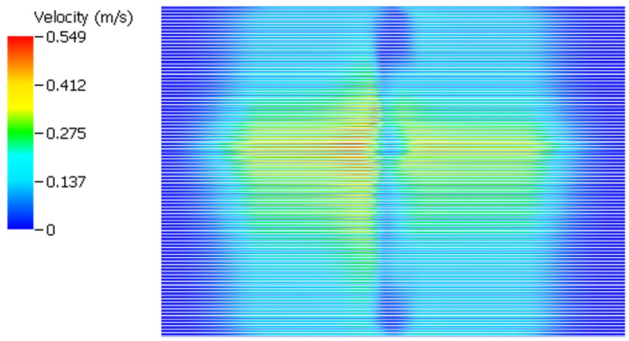

Fig. 14 Velocity profile inside parallel channels at half the fin height and 1 LPM

the case thermal resistance and pressure drop of the electroless nickel-plated cold plate as well as those of previously tested cold plates with various designs and materials. The impinging single-phase cold plates show lower pressure drops than others at the specified flow rate of 1 LPM. The CNC cold plate shows lower case thermal resistance than other industry copper cold plates. The thermal resistance caused by TIM is taken into account. To provide a fair comparison, the thermal resistance of PCM TIM is added to the reported cold plate thermal resistances. The superior thermal performance of the CNC cold plate can be explained by the compact fin size and the thin base thickness. In most liquid-cooled cold plates, the base makes the highest contribution to the total thermal resistance. The current cold plate has a very thin (0.07 mm) base thickness, which contributes a small amount to the total case thermal resistance. This cold plate is a great candidate for high-density and large-scale applications, wherein high thermal capacity and corrosion resistance are needed. However, the thinner the base thickness is, the higher the thermal gradient at the case surface will be. This could be a limitation for nonuniform heat flux applications, wherein heat spreading from hot spots to low heat density areas is necessary. In general, the proper choice of a liquid cooling cold plate can extend the single-phase cooling limits and overall system efficacy.

6 Conclusion

Cold plates are one of the most critical components in liquid cooled data centers. With that in mind, this study focused on the cooling performance of a novel electroless nickel-plated corrosion resistant CNC manufactured cold plate. The thermohydraulic performance of the CNC electroless nickel-plated impinging cold plate was investigated using an experimental test setup with a mock processing unit to examine processor level heat flux and compare it to that of a pure copper cold plate. A CFD analysis was done to capture the temperature profile and nonuniformity of the case surface. The study acquired accurate performance curves for the cold plate, which can be used in a server level analysis. Overall, the results showed that:

- The hydraulic performance of the nickel-plated cold plate is identical to the pure copper cold plate.
- Plating nickel on a pure copper cold plate slightly increases the case temperature and thereby the thermal resistance. The thermal resistance of nickel-plated is slightly higher (~1%) than pure copper one at 32 °C inlet temperature and 1 LPM flow rate.
- A higher liquid inlet temperature is more favorable in data centers because a lower pressure drop and reduced thermal resistance contribute to power savings in the chiller.
- The case temperature profile will become more uniform by increasing the flow rate because of a smaller temperature gradient between the inlet and outlet area.
- The design of the inlet and outlet ports is an important consideration, as it will affect the hydraulic and thermal nonuniformity. The inlet and outlet ports should be designed to maintain the minimum hydraulic and thermal non-uniformity
- The proper design and choice of manufacturing methods improve the cold plates' overall performance and overall system efficiency. The comparison of other cold plates reported in the literature to the novel cold plate in this study confirms that its cooling performance is superior.
- Overall, the electroless nickel plating on the pure copper heat sink had a negligible effect on the thermal performance of the cold plate. This indicates that nickel plating is a great candidate for liquid cooling environments where corrosion is a concern.

Table 4 Comparison results of this study CNC design to other reported cold plates

Authors/year	Design description	Test boundary condition	R_{th}^{case} (K cm^2/W) at 1 LPM	ΔP (psi)
This study design	CNC manufactured, Impinging copper microchannel cold plate	DI water/indirect single phase liquid cooling	0.232	0.54
Hadad et al. [20]	Skived, impinging microchannel copper cold plate	DI water/indirect single phase liquid cooling	0.301	0.17
Refai-Ahmed et al. [35]	Skived, parallel microchannel copper cold plate	PG25/indirect single phase liquid cooling	0.40	—
Ramakrishnan et al. [36]	Skived, parallel microchannel cold plate for multichip copper cold plate	DI water/indirect single phase liquid cooling	0.38	0.97
Ramakrishnan et al. [36]	Skived, impinging microchannel cold plate multichip copper cold plate	DI water/indirect single-phase liquid cooling	0.37	0.85
Ramakrishnan et al. [36]	Skived, parallel discrete microchannel multichip copper cold plate	DI water/indirect single-phase liquid cooling	0.36	0.88
Hoang et al. [9,10]	Skived, multi-impinging microchannel copper cold plate	HFE 7000/indirect two-phase liquid cooling	0.481	1.74
Hoang et al. [37]	Skived, impinging grooved microchannel copper cold plate	HFE 7000/ Indirect two-phase liquid cooling	0.26	2.6
Zhang et al. [38]	Skived, aluminum parallel microchannel heat sink	/Indirect single phase liquid cooling	0.46	~1.33
Acikalin and Schroedera [39]	Skived, A prototype microchannel multijet module	Water/direct single-phase	0.27	5

Acknowledgment

Many thanks to Firas W. Alshatnawi and Dr. Mark Poliks for their help with SEM images. We would also like to show our gratitude to Mark Seymour and Future Facilities for their continuous support. B.S. acknowledges the NSF Award IIP-1738793 and the Integrated Electronics Engineering Center (IEEC) at the State University of New York at Binghamton. The IEEC is a New York State Center for Advanced Technology with funding from New York State through the Empire State Development Corporation.

Funding Data

- NSF (Award IIP-1738793; Funder ID: 10.13039/100000001).

Nomenclature

A = area (m^2)
H = distance between two K-type thermocouples (m)
K = thermal conductivity ($J/m\,K$)
P = pressure (Pa)
$\dot{q}$ = chip power (W)
Q = coolant volumetric flow rate (m^3/s)
R = thermal resistance ($K\,m^2/W$)
T = temperature (K)

Greek Symbols

δ = uncertainty in the equation
ψ = case temperature non-uniformity

Subscripts

ave = average
bot = bottom
e = external
i = internal
in = inlet
J = junction
t = conductive
th = thermal
TIM = thermal interface material

References

[1] Kadam, S. T., and Kumar, R., 2014, "Twenty First Century Cooling Solution: Microchannel Heat Sinks," Int. J. Therm. Sci., **85**, pp. 73–92.
[2] Lawrence, A., 2020, "Rack Density is Rising," Uptime Institute Blog, New York.
[3] El-Sayed, N., Stefanovici, I. A., Amvrosiadis, G., Hwang, A. A., and Schroeder, B., 2012, "Temperature Management in Data Centers: Why Some (Might) Like It Hot," Sigmetrics Perform. Eval. Rev., **40**(1), pp. 163–174.
[4] Greenberg, S., Mills, E., Tschudi, B., Rumsey, P., Engineers, R., and Myatt, B., 2006, "Best Practices for Data Centers: Lessons Learned From Benchmarking 22 Data Centers," ACEEE Summer Study on Energy Efficiency in Buildings, p. 12.
[5] Hadad, Y., Pejman, R., Ramakrishnan, B., Chiarot, P. R., and Sammakia, B. G., 2018, "Geometric Optimization of an Impinging Cold-Plate With a Trapezoidal Groove Used for Warm Water Cooling," 17th IEEE Intersociety Conference on Thermal and Thermomechanical Phenomena in Electronic Systems (ITherm), San Diego, CA, May 29–June 1, pp. 673–682.
[6] Copeland, D. W., 1995, "Manifold Microchannel Heat Sinks: Analysis and Optimization," Therm. Sci. Eng., **34**, pp. 7–12.
[7] Copeland, D. W., Takahira, H., Nakayama, W., and Bock-Choon, P., 1995, "Manifold Microchannel Heat Sinks: Theory and Experiment," Therm. Sci. Eng., **34**, pp. 9–15.
[8] Hadad, Y., Radmard, V., Rangarajan, S., Farahikia, M., Refai-Ahmed, G., Chiarot, P. R., and Sammakia, B., 2021, "Minimizing the Effects of on-Chip Hotspots Using Multi-Objective Optimization of Flow Distribution in Water-Cooled Parallel Microchannel Heatsinks," ASME J. Electron. Packag., **143**(2), p. 021007.
[9] Hoang, C. H., Rangarajan, S., Khalili, S., Ramakrisnan, B., Radmard, V., Hadad, Y., Schiffres, S., and Sammakia, B., 2021, "Hybrid Microchannel/Multi-Jet Two-Phase Heat Sink: A Benchmark and Geometry Optimization Study of Commercial Product," Int. J. Heat Mass Transfer, **169**, p. 120920.
[10] Hoang, C. H., Khalili, S., Ramakrisnan, B., Rangarajan, S., Hadad, Y., Radmard, V., Sikka, K., Schiffres, S., and Sammakia, B., 2020, "An Experimental Apparatus for Two-Phase Cooling of High Heat Flux Application Using an Impinging Cold Plate and Dielectric Coolant," 36th Semiconductor Thermal Measurement, Modeling Management Symposium (SEMI-THERM), San Jose, CA, Mar. 16–20, pp. 32–38.
[11] Wiriyasart, S., and Naphon, P., 2019, "Liquid Impingement Cooling of Cold Plate Heat Sink With Different Fin Configurations: High Heat Flux Applications," Int. J. Heat Mass Transfer, **140**, pp. 281–292.
[12] Qu, W., and Mudawar, I., 2002, "Analysis of Three-Dimensional Heat Transfer in Micro-Channel Heat Sinks," Int. J. Heat Mass Transfer, **45**(19), pp. 3973–3985.
[13] Qu, W., and Mudawar, I., 2002, "Experimental and Numerical Study of Pressure Drop and Heat Transfer in a Single-Phase Micro-Channel Heat Sink," Int. J. Heat Mass Transfer, **45**(12), pp. 2549–2565.
[14] Xie, X. L., Liu, Z. J., He, Y. L., and Tao, W. Q., 2009, "Numerical Study of Laminar Heat Transfer and Pressure Drop Characteristics in a Water-Cooled Minichannel Heat Sink," Appl. Therm. Eng., **29**(1), pp. 64–74.
[15] Chai, L., Xia, G. D., and Wang, H. S., 2016, "Parametric Study on Thermal and Hydraulic Characteristics of Laminar Flow in Microchannel Heat Sink With Fan-Shaped Ribs on Sidewalls—Part 2: Pressure Drop," Int. J. Heat Mass Transfer, **97**, pp. 1081–1090.
[16] Hadad, Y., Ramakrishnan, B., Pejman, R., Rangarajan, S., Chiarot, P. R., Pattamatta, A., and Sammakia, B., 2019, "Three-Objective Shape Optimization and Parametric Study of a Micro-Channel Heat Sink With Discrete Non-Uniform Heat Flux Boundary Conditions," Appl. Therm. Eng., **150**, pp. 720–737.
[17] Radmard, V., Hadad, Y., Rangarajan, S., Hoang, C. H., Fallahtafti, N., Arvin, C. L., Sikka, K., Schiffres, S. N., and Sammakia, B. G., 2021, "Multi-Objective Optimization of a Chip-Attached Micro Pin Fin Liquid Cooling System," Appl. Therm. Eng., **195**, p. 117187.
[18] Radmard, V., Hadad, Y., Azizi, A., Rangarajan, S., Hoang, C. H., Arvin, C., Sikka, K., Schiffres, S. N., and Sammakia, B., 2020, "Direct Micro-Pin Jet Impingement Cooling for High Heat Flux Applications," 36th Semiconductor Thermal Measurement, Modeling Management Symposium (SEMI-THERM), San Jose, CA, Mar. 16–20, pp. 1–9.
[19] Radmard, V., Azizi, A., Rangarajan, S., Fallahtafti, N., Hoang, C. H., Mohsenian, G., Nemati, K., Schiffres, S. N., and Sammakia, B., 2021, "Performance Analysis of Impinging Chip-Attached Micro Pin Fin Direct Liquid Cooling Package for Hotspot Targeted Applications," 20th IEEE Intersociety Conference on Thermal and Thermomechanical Phenomena in Electronic Systems (ITherm), San Diego, CA, June 1–4, pp. 220–228.
[20] Hadad, Y., Fallahtafti, N., Choobineh, L., Hoang, C. H., Radmard, V., Chiarot, P. R., and Sammakia, B., 2020, "Performance Analysis and Shape Optimization of an Impingement Microchannel Cold Plate," IEEE Trans. Compon., Packag. Manuf. Technol., **10**(8), pp. 1304–1319.
[21] Hadad, Y., Ramakrishnan, B., Alkharabsheh, S., Chiarot, P. R., and Sammakia, B., 2017, "Numerical Modeling and Optimization of a V-Groove Warm Water Cold-Plate," 33rd Thermal Measurement, Modeling Management Symposium (SEMI-THERM), San Jose, CA, Mar. 13–17, pp. 314–319.
[22] Kisitu, D., and Ortega, A., 2021, "Thermal-Hydraulic Analytical Models of Split-Flow Microchannel Liquid-Cooled Cold Plates With Flow Impingement," ASME Paper No. IPACK2021-73283.
[23] Escher, W., Michel, B., and Poulikakos, D., 2010, "A Novel High Performance, Ultra Thin Heat Sink for Electronics," Int. J. Heat Fluid Flow, **31**(4), pp. 586–598.
[24] Addagatla, A., Fernandes, J., Mani, D., Agonafer, D., and Mulay, V., 2015, "Effect of Warm Water Cooling for an Isolated Hybrid Liquid Cooled Server," 31st Thermal Measurement, Modeling Management Symposium (SEMI-THERM), San Jose, CA, Mar. 15–19, pp. 203–207.
[25] Hackerman, N., 2002, "Effect of Temperature on Corrosion of Metals by Water," ACS Publications, Washington, DC, accessed Aug. 31, 2021, https://pubs.acs.org/doi/pdf/10.1021/ie50512a020
[26] Kim, C.-U., and Chang, J.-Y., 2017, "Corrosion in a Closed-Loop Electronic Device Cooling System With Water as Coolant and Its Detection," 16th IEEE Intersociety Conference on Thermal and Thermomechanical Phenomena in Electronic Systems (ITherm), Orlando, FL, May 30–June 2, pp. 558–564.
[27] Yaser Yons - Academia.Edu, 2021, "(PDF) Corrosion Engineering: Principles and Practice," Yaser Yons - Academia.Edu, accessed July 20, 2022, https://books.google.com/books/about/Corrosion_Engineering.html?id=Zl2XlEOuJnMC
[28] Chirkunov, A., and Kuznetsov, Y., 2015, "Chapter 4 - Corrosion Inhibitors in Cooling Water Systems," Miner. Scales and Deposits, pp. 85–105.
[29] Loto, C. A., 2016, "Electroless Nickel Plating – A Review," Silicon, **8**(2), pp. 177–186.
[30] Shia, D., Yang, J., Sivapalan, S., Soeung, R., and Amoah-Kusi, C., 2021, "Corrosion Study on Single-Phase Liquid Cooling Cold Plates With Inhibited Propylene Glycol/Water Coolant for Data Centers," ASME J. Manuf. Sci. Eng., **143**(11), p. 111012.
[31] Mohapatra, A. C., 2006, "An Overview of Liquid Coolants for Electronics Cooling," Electronics Cooling, accessed July 20, 2022, https://www.electronics-cooling.com/2006/05/an-overview-of-liquid-coolants-for-electronics-cooling/
[32] Ellsworth, M. J., 2006, "Comparing Liquid Coolants From Both A Thermal And Hydraulic Perspective," Electronics Cooling, accessed July 20, 2022, https://www.electronics-cooling.com/2006/08/comparing-liquid-coolants-from-both-a-thermal-and-hydraulic-perspective/
[33] Techstreet Store, Techstreet LLC, 2021, "Liquid Cooling Guidelines for Datacom Equipment Centers," 2nd ed., Techstreet LLC, Chicago, IL, accessed

Nov. 13, 2021, https://www.techstreet.com/ashrae/standards/liquid-cooling-guidelines-for-datacom-equipment-centers-2nd-ed?ashrae_auth_token=&gateway_code=ashrae&product_id=1873288
[34] Future Facilities, 2021, "Home | 6SigmaET by Future Facilities—Thermal Simulation of Electronics," Future Facilities, San Jose, CA, accessed Apr. 28, 2021, https://www.6sigmaet.info/
[35] Refai-Ahmed, G., Do, H., Hadad, Y., Rangarajan, S., Sammakia, B. G., Gektin, V., and Cader, T., 2020, "Establishing the Single-Phase Cooling Limit for Liquid-Cooled High Performance Electronic Devices," 22nd Electronics Packaging Technology Conference (EPTC), Singapore, Dec. 2–4, pp. 340–346.
[36] Ramakrishnan, B., Tradat, M., Hadad, Y., Ghose, K., and Sammakia, B., 2019, "Characterization of Liquid Cooled Cold Plates for a Multi Chip Module (MCM) and Their Impact on Data Center Chiller Operation," IEEE 17th International Conference on Industrial Informatics (INDIN), Helsinki, Finland, July 22–25, pp. 1419–1424.
[37] Hoang, C. H., Rangarajan, S., Radmard, V., Fallahtafti, N., Tradat, M., Arvin, C., Schiffres, S., and Sammakia, B., 2021, "Two-Phase Impingement Cooling Using a Trapezoidal Groove Microchannel Heat Sink and Dielectric Coolant HFE 7000," 20th IEEE Intersociety Conference on Thermal and Thermomechanical Phenomena in Electronic Systems (ITherm), San Diego, CA, June 1–4, pp. 237–245.
[38] Zhang, H. Y., Pinjala, D., Wong, T. N., Toh, K. C., and Joshi, Y. K., 2005, "Single-Phase Liquid Cooled Microchannel Heat Sink for Electronic Packages," Appl. Therm. Eng., **25**(10), pp. 1472–1487.
[39] Acikalin, T., and Schroeder, C., 2014, "Direct Liquid Cooling of Bare Die Packages Using a Microchannel Cold Plate," 14th Intersociety Conference on Thermal and Thermomechanical Phenomena in Electronic Systems (ITherm), Orlando, FL, May 27–30, pp. 673–679.